

Gamma-ray Observations of the Galactic Plane at Energies $E > 500$ GeV

S.LeBohec¹, I.H.Bond², S.M.Bradbury², J.H.Buckley³, A.M.Burdett^{2,4}, D.A.Carter-Lewis¹,
M.Catanese⁴, M.F.Cawley⁵, S.Dunlea⁶, M. D'Vali², D.J.Fegan⁶, S.J.Fegan⁴, J.P.Finley⁷,
J.A.Gaidos⁷, T.A.Hall⁷, A.M.Hillas², D.Horan^{4,6}, J.Knapp², F.Krennrich¹, R.W.Lessard⁷, D.
Macomb⁸, C.Masterson⁶, J.Quinn⁶, H.J.Rose², F.W.Samuelson¹, G.H.Sembroski⁷, V.V.Vassiliev⁴,
T.C.Weekes⁴

ABSTRACT

In 1998 and 1999 the Whipple Observatory 10 m telescope was used to search for diffuse gamma ray emission from the Galactic Plane. At this time, the telescope was equipped with a large (4.8°) field of view camera, well suited to detect diffuse γ -ray emission. No significant evidence of emission was found. Assuming the TeV emission profile matches EGRET observations above 1 GeV with a differential spectral index of 2.4, we derive an upper limit of $3.0 \cdot 10^{-8} \text{ cm}^{-2} \text{ s}^{-1} \text{ sr}^{-1}$ for the average diffuse emission above 500 GeV in the galactic latitude range from -2° to $+2^\circ$ at galactic longitude 40° . Comparisons with EGRET observations provide a lower limit of 2.31 for the differential spectral index of the diffuse emission, assuming there is no break in the spectrum between 30 GeV and 500 GeV. This constrains models for diffuse emission with a significant inverse Compton contribution.

Subject headings: cosmic rays, diffuse γ -ray galactic emission — gamma rays: observations

¹Department of Physics and Astronomy, Iowa State University, Ames, IA 50011-3160

²Department of Physics, University of Leeds, Leeds, LS2 9JT, Yorkshire, England, UK

³Department of Physics, Washington University, St. Louis, MO 63130, USA

⁴Fred Lawrence Whipple Observatory, Harvard-Smithsonian CfA, P.O. Box 97, Amado, AZ 85645-0097

⁵Physics Department, St.Patrick's College, Maynooth, County Kildare, Ireland

⁶Physics Department, University College, Dublin 4, Ireland

⁷Department of Physics, Purdue University, West Lafayette, IN 47907

⁸Laboratory for High-Energy Astrophysics, NASA/GSFC, Greenbelt, MD 20771 and Universities Space Research Association, Lanham MD

1. Introduction

High energy γ -rays traverse the Galaxy without significant attenuation, and hence diffuse γ -ray emission probes the galaxy as a whole. As was observed with OSO-3 (Kraushaar et al. 1972), emission from the galactic plane is the main feature of the high energy γ -ray sky. Observations with the SAS-2 and COS-B satellites showed this emission was generally correlated with the spatial structures in the Galaxy seen at other wavelengths (Fichtel et al. 1975; Hartman et al. 1979; Mayer-Hasselwander et al. 1980). The greater sensitivity and angular resolution of the EGRET instrument (Hughes et al. 1980; Kanbach et al. 1988; Kanbach et al. 1989) provided a much more detailed spectral and spatial picture of the diffuse emission from the Galaxy (Hunter et al. 1997).

The spectral and spatial distributions of diffuse high energy emission can be interpreted using a detailed model (Bertsch et al. 1993) of the emission. This model is based on γ -ray production by nucleon-nucleon and electron (bremsstrahlung and inverse Compton) scattering in the interstellar medium. The matter and photon distributions in the interstellar medium are inferred from radio, infrared, visible and ultra-violet observations. The cosmic rays are assumed to have the same composition and spectrum everywhere in the galaxy with a density that is correlated with the matter density. The model precisely reproduces the spatial and spectral data from EGRET up to energies of 100 MeV. However, for $E > 1$ GeV the predicted flux is 40% lower than observations indicate (Hunter et al. 1997).

Pohl and Esposito (1998) explained the observed excess at $E > 1$ GeV as inverse Compton (IC) emission by a cosmic-ray electron injection spectrum harder than that used by Hunter et al. (1997). The latter assumed a spectral index of 2.4, which was inferred from the local cosmic-ray electron spectrum when propagated through the galaxy. If shock acceleration in supernova remnants (SNRs) produces the electrons, a spectral index closer to 2.0 is expected. Furthermore, most SNRs have power law spectra at radio wavelengths with $\alpha \sim 0.5$ (Green et al. 1995), indicating injection spectra with index near 2.0. Pohl and Esposito (1998) showed that a change of spectral index of only 0.4 is sufficient to account for the observed excess. Indeed, it has been previously argued that if the electron cutoff energy is high enough, IC emission may be the dominant source of diffuse γ -rays at TeV energies (Porter & Protheroe 1997). Pohl and Esposito (1998) suggest that the discrepancy with the local electron spectrum is a statistical fluctuation: high energy cosmic-ray electrons tend to have a local origin because bremsstrahlung and IC energy losses prevent propagation over large distance. Therefore, they are subject to Poisson fluctuations in the number of supernovae accelerating electrons at a given time, whereas the unattenuated γ -rays originate from broader parts of the Galaxy and reflect an electron spectral index closer to the galactic average. In examining possible mechanisms for the EGRET excess, Moskalenko and Strong (2000) and Strong, Moskalenko and Reimer (1999, 2000) apply several detailed models to the full spectrum of diffuse gamma-ray emission from the Galaxy. These authors also conclude that IC emission from a hardened electron injection spectrum (< 2) is the favored origin of the high energy EGRET excess.

We have searched for diffuse emission from the Galactic Plane at higher energies than detected by EGRET using the Whipple Observatory 10 m imaging atmospheric Cherenkov telescope to observe the galactic plane region at ($b = 0^\circ$, $l = 40^\circ$). Although a simple extrapolation of the highest energy EGRET spectrum indicates the diffuse emission should be detectable, no signal was found. Using an analysis method specifically developed for this measurement we derive upper limits on the galactic diffuse γ -ray emission at $E > 500$ GeV. We compare this result to a power law extrapolation of EGRET's spectral points above 1 GeV and derive a lower limit on the spectral index. In sections 2 and 3 the observations and data analysis are described. In section 4, the results are presented and discussed in the context of the EGRET results summarized above.

2. Observations

The observations were made with the Whipple Observatory atmospheric Cherenkov imaging telescope as described in Cawley et al. (1990). The telescope is located at an altitude of 2300m and consists of a 10 m diameter optical reflector with a fast photomultiplier tube (PMT) camera in the focal plane. For point sources, the image shapes and orientations can be used to distinguish γ -ray images from a much larger number of cosmic-ray hadron images (Hillas et al. 1985). The camera can also be used to map an extended portion of the sky (Lessard et al. 1997). The observations presented here were obtained using a 331 PMT camera with spacing of 0.24° covering a field of view of 4.8° .

The observations of the galactic plane were centered on coordinates ($l = 40^\circ$, $b = 0^\circ$), which is within the inner region of the galaxy where the diffuse emission is most intense. This region culminates at the relatively small zenith angle 25° at the Observatory and so gives a fairly low energy threshold. The field was also selected for its lack of bright stars which allows sensitive atmospheric Cherenkov radiation measurement.

The observations were carried out in a standard ON-OFF mode in which the galactic plane (ON) is tracked for 28 minutes after which the telescope tracks a background region (OFF) covering the same path in elevation and azimuth for another 28 minutes. Some of the OFF data were measured before the ON data. During the observations, several PMTs were switched off in both ON and OFF data set because of light from bright stars.

In 1998, the telescope was triggered when any two out of the 331 PMTs exceeded a threshold corresponding to ~ 65 photoelectrons. From Monte Carlo simulations we found that, if analyzed as describe below, the 1998 data had an energy threshold of 700 GeV. In 1999 a topological (pattern) trigger was used requiring triggering PMTs to be neighbors (Bradbury, et al. 1999), and we reduced the threshold to 500 GeV. (Here, the telescope energy threshold is defined as the energy for which the count rate peaks for a power-law spectrum with differential index 2.4). The data consists of 7 ON-OFF pairs obtained in 1998 and 10 ON-OFF pairs in 1999.

3. Data analysis

In this section we describe the main four steps in the analysis, starting with the γ -ray candidate selection (step 1) and angular origin reconstruction (step 2). For this particular analysis we also had to correct for sensitivity inhomogeneities across the field (step 3). This allowed us to fit a specific pattern corresponding to diffuse emission in the final data (step 4).

3.1. Gamma-ray candidate selection

Software “padding” (Cawley 1993) is used to compensate for differences in noise level in the ON and OFF runs. The image is also “cleaned” (Reynolds et al. 1993) to alleviate the noise effects of pixels that are not part of the shower image. The image is then characterized by the image parameters calculated from the 1st, 2nd and 3rd moments of the recorded light distribution (see Figure 1). The image parameters are *Length*, *Width*, *Distance* from the center of the field of view and *Asymmetry* as described in Fegan et al. (1997). The γ -ray images tend to be comet-shaped, with *Asymmetry* indicating the development direction of the shower. At least 78 and 56 photoelectrons were required in the two brightest pixels of each image to ensure that it is well above background noise. The *Distance* of the image centroid from the center of the field of view was restricted to be less than 1.8° to ensure that the entire image is contained in the camera. Boundary values for the *Length* and *Width* parameters were derived by maximizing the significance of the Crab Nebula observations obtained with this camera. These selection criteria for γ -ray candidates are summarized in Table 1. Since the telescope is being used to image an extended portion of the sky, no orientation selection is made.

3.2. Reconstruction of the arrival direction

For each selected γ -ray candidate, the most likely point of origin is reconstructed (see Figure 1) by applying the following method (Lessard et al. 1997) which was tested and optimized on off-center Crab Nebula observations:

- the source is assumed to lie on the shower image major axis,
- the source is assumed to be in the direction indicated by the *Asymmetry* parameter, and
- the source is assumed to be located $1.85^\circ(1 - Width/Length)$ from the image centroid.

The first criterion results from the fact that the image axis is the projection in the focal plane of the shower axis which points toward the source. The *Asymmetry* parameter allows the identification of the top and the bottom of the shower. The third criteria is empirical but intuitive. The image elongation (measured by $1 - Width/Length$) and its distance from the source both increase with the shower impact parameter. The standard deviation of the point spread function provided by this method is 0.12° .

3.3. Sensitivity correction across the field

As one moves from the center of the field of view, the sensitivity decreases because the outermost portions of the images may be missed. In addition, since pixels were turned off because of stars, the sensitivity profile has irregularities. We have developed the following calibration procedure to compensate for the variation of sensitivity across the field of view.

A uniform distribution of TeV γ -rays was simulated. The selection criteria from section 3.1 were applied. Figure 2 shows the radial distribution of the reconstructed source position which is well fit by a centered two-dimensional Gaussian with a standard deviation of 1.2° . We have verified this sensitivity pattern at two points using Crab Nebula data taken off axis. We then used background events that pass our selection criteria to measure $S_{correct}$, the discrepancy ratio between the simulated and real field sensitivity functions. The $S_{correct}$ factor map obtained for the 1999 galactic plane observations is shown in Figure 3. Correction factors can be as large as 2. In the subsequent analysis, each event has a weight equal to the $1/S_{correct}$ factor corresponding to the reconstructed direction of origin in the camera frame. This correction allows us to directly compare the simulated diffuse emission with the recorded data.

3.4. Galactic diffuse emission flux measurement

In this analysis, we assume that the diffuse emission is uniform along the galactic equator over our field of view. The latitude profile has been taken from EGRET observations above 1 GeV as shown in Figure 4, where the smooth curve indicates how the profile was modeled. We have used simulations to estimate the response of the camera to this emission profile assuming a power law energy spectrum with a differential spectral index of 2.4. As one moves across the camera in the direction of galactic longitude, the number of γ -rays detected should remain constant for an ideal camera. However, because of the finite field of view, the detection efficiency falls off toward the edge. Consequently, we have restricted the data to longitudes between 38.5° and 41.5° (left side of Figure 5). The resulting latitude profile as it should appear in our data is shown on the right side of Figure 5. The smooth curve shows how it was modeled when fit to our data with amplitude as the only free parameter.

4. Results

The analysis described above was applied to the data accumulated in 1998 and 1999. The latitude profile derived from the simulation of the diffuse emission was fitted to both the 1998 and 1999 data with results shown in Figure 6. Although the 1998 data exhibited a 3.2σ excess $((1.84^{+0.57})\gamma/\text{minute})$, the 1999 data is consistent with a null result $((0.42^{+0.43})\gamma/\text{minute})$, and, from both datasets we derive upper limits on the average diffuse emission flux in the portion of

sky defined by $38.5^\circ < l < 41.5^\circ$ and $2^\circ < b < 2^\circ$. Assuming a differential spectral index $\gamma = 2.4$, we obtained a 99.9% confidence level upper limit on the flux of $6.3 \cdot 10^{-8} \text{s}^{-1} \text{cm}^{-2} \text{sr}^{-1}$ for 1998 with a threshold of 700 GeV and $3.0 \cdot 10^{-8} \text{s}^{-1} \text{cm}^{-2} \text{sr}^{-1}$ for 1999 with a threshold of 500 GeV.

In Figure 7, simple power law spectra corresponding to the upper limits using several values of spectral index are compared to the high end of the spectrum obtained with EGRET for the same portion of sky. Our results are not compatible with an extrapolation of the EGRET measurements assuming a hard spectrum. This is quantified in Figure 8 which shows the 99.9% and 99% confidence level upper limits on the diffuse emission flux above 500 GeV as a function of the assumed spectral index. It is compared to the simple power law extrapolation to $E > 500$ GeV of the EGRET measurement above 1 GeV for the same field. This comparison leads to a lower limit on the differential spectral index of 2.31 at the 99.9% confidence level.

5. Concluding Remarks

The observations of the galactic plane did not yield a detection of the diffuse emission, and we derived an upper limit of $3.0 \cdot 10^{-8} \text{s}^{-1} \text{cm}^{-2} \text{sr}^{-1}$ for the flux above 500 GeV in the portion of galactic plane defined by $38.5^\circ < l < 41.5^\circ$ and $2^\circ < b < 2^\circ$, assuming a differential spectral index of 2.4. We showed that these upper limits imply that the diffuse emission cannot extend up to 500 GeV with a simple power law with a differential spectral index smaller than 2.31.

These observations are compatible with earlier observations made in the drift-scan mode with the 10m reflector (Reynolds et al. 1993; Reynolds et al. 1990). Other constraints on the extrapolation of the diffuse emission spectrum to greater energies than observed by EGRET, arise from observations with extensive air shower detectors like TIBET above 10 TeV (Amenomori et al. 1997), EAS-TOP (Aglietta et al. 1993) and CASA MIA (Borione et al. 1998) above 130 TeV. Among these experiments, TIBET, the closest one to us on the energy scale, also concentrated on the portion of sky defined by $20^\circ < l < 55^\circ$ and $-5^\circ < b < +5^\circ$ including the field we observed. These observations provided similar limits on the spectral index as presented here but the energies being probed are larger by at least one order of magnitude.

In the Hunter et al. (1997) model, a value of ~ 2.3 for the inverse Compton spectrum for the upper end (50 GeV) of the EGRET spectrum is found from Fig. 4 of their paper. This model assumes a SNR electron injection spectral index of 2.4, and the inverse Compton gamma-ray spectral index is marginally consistent with our lower limit. However, the model does not fit the high end of the EGRET spectrum. Pohl and Esposito (1998) explain the excess above 1 GeV as due to inverse Compton emission in a model using electrons injected into the galaxy from SNR with a harder power-law spectrum with an index of 2. However, their inverse Compton spectrum gives a differential spectral index of ~ 1.85 , in contradiction our limit of 2.31. In extrapolating to energies of 500 GeV, there may be some softening of the inverse Compton spectrum due to the onset of Klein-Nishina reduction in scattering cross section. Nevertheless the Cosmic Background

Radiation should be a large part of the target photon population, and the corresponding portion of the inverse Compton spectrum would not be significantly affected until the γ -rays reach energies well above 500 GeV. Thus our limits should constrain such models (e.g., Pohl and Esposito, 1998; Strong, Moskalenko and Reimer, 2000) possibly implying a break in the primary electron spectrum.

We acknowledge the technical assistance of K. Harris and E. Roach. This research is supported by grants from the U.S. Department of Energy and by PPARC in the UK and by Forbairt in Ireland.

REFERENCES

- Aglietta, M., et al. 1993, ApJ, 397, 148
- Amenomori, M., et al. 1997, Proc. 25th Int. Cosmic Ray Conf. (Durban), 3, 117
- Borione, A., et al. 1998, ApJ, 493, 175
- Bertsch, D.L., et al. 1993, ApJ, 481, 205–240
- Bradbury, S.M., et al., 1999, Proc. 26th Int. Cosmic Ray Conf. (Salt Lake City), 5, 263.
- Cawley, M.F., et al. 1990, Experimental Astronomy, 1, 173
- Cawley, M.F. 1993 in Toward a Major Atmospheric Cherenkov Detector II (Calgary), ed. R.C.Lamb, 176
- Fegan, D. 1997, J.Phys.G, 23, 1013
- Fichtel C. et al. 1975, ApJ, 198, 163
- Green D.A. 1995, “A catalogue of Galactic SNR”, Mullard RAO, Cambridge, UK
- Hartman, R., et al. 1979, ApJ, 230, 597
- Hillas, A.M., et al. 1985, Proc. 19th Int. Cosmic Ray Conf. (LaJolla), 3, 445
- Hughes, E.B., et al. 1980, IEEE Trans. Nucl. Sci., NS-27, 364
- Hunter, S.D., et al. 1997, ApJ, 416, 587–600
- Kanbach, G., et al. 1988, Space Science Review, 49, 69
- Kanbach, G., et al. 1989, in Proc. Gamma Ray Observatory Science Work Shop, ed. W.N.Johnson, (Greenbelt: NASA), 2-1
- Kraushaar, W., et al. 1972, ApJ, 177, 341
- Lessard, R.W., et al. 1997, Proceed. of “Toward a Major Atmospheric detector V”, (Kruger Park), ed. O.C. De Jager, 356
- Mayer-Hasselwander, H., et al. 1980, in Ann. NY Acad. Sci. 336, Ninth Texas Symp. on Relativistic Astrophysics, 211
- Mayer-Hasselwander, H., et al. 1982, A&A, 105, 164
- Moskalenko, I. V. and Strong, A.W. 2000, ApJ, 528, 357
- Pohl, M. and Esposito, J.A. 1998, ApJ, 507, 327–338

Porter, T.A., and Protheroe, R.J. 1997, *J.Phys.G*, 23, 1765

Reynolds, P.T., et al. 1990, *Proc. 21st Int. Cosmic Ray Conf. (Adelaide)*, 2, 383

Reynolds, P.T., et al. 1993, *ApJ*, 404, 206.

Sommers, P., & Elbert, J.W., 1987, *J.Phys.G: Nucl.Phys.*, 13, 553

Strong, A.W., Moskalenko and Reimer, O., I. V. 1999, *astro-ph/9912102*

Strong, A.W., Moskalenko and Reimer, O., I. V. 2000, to be published in *ApJ*, 537

Table 1. γ -ray candidate selection.

Selection criteria
$Max1 > 78$ d.c.
$Max2 > 56$ d.c.
$0.073^\circ < Width < 0.16^\circ$
$0.16^\circ < Length < 0.43^\circ$
$Distance < 1.8^\circ$

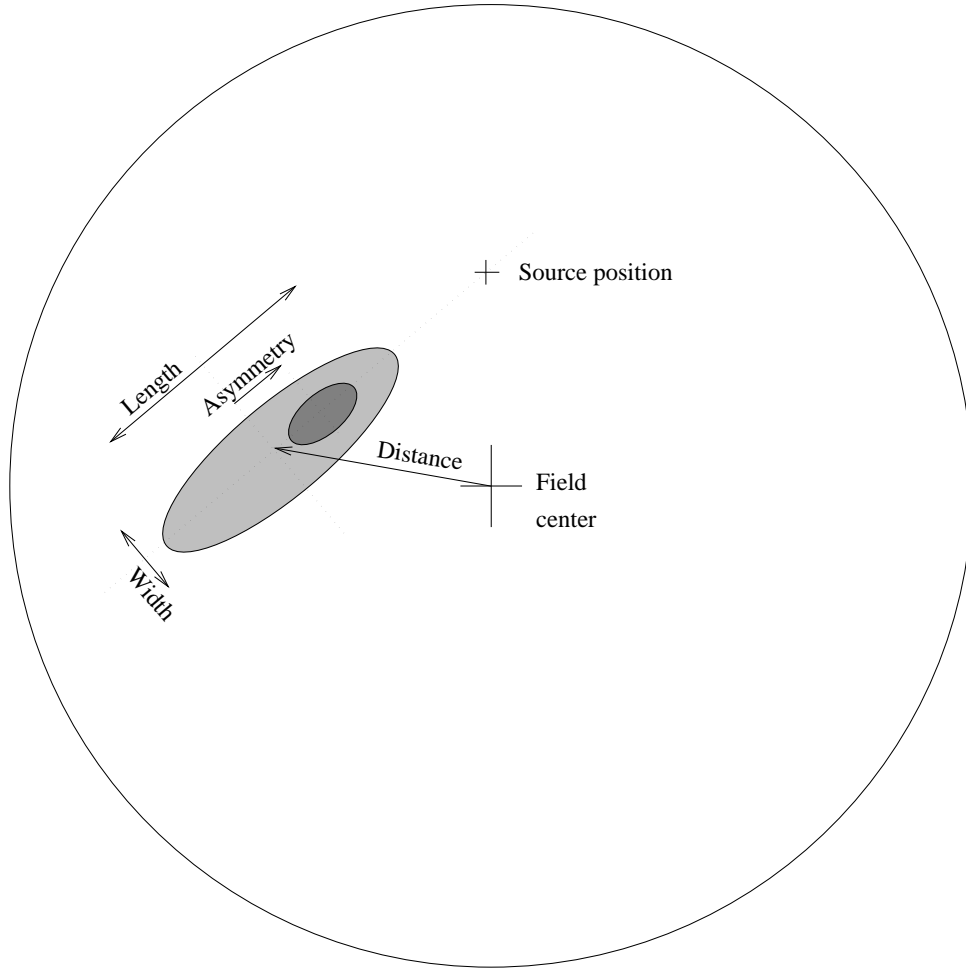


Fig. 1.— The elliptical image is first characterized by its position and orientation. The *Length* and *Width* allow the preferential selection of γ -ray shower images which tend to be more elongated than the bulk of cosmic-ray shower images. The asymmetry in the distribution of light along the major axis can be characterized by the *Asymmetry* parameter and indicates the direction of the top of the shower and therefore points to the source direction.

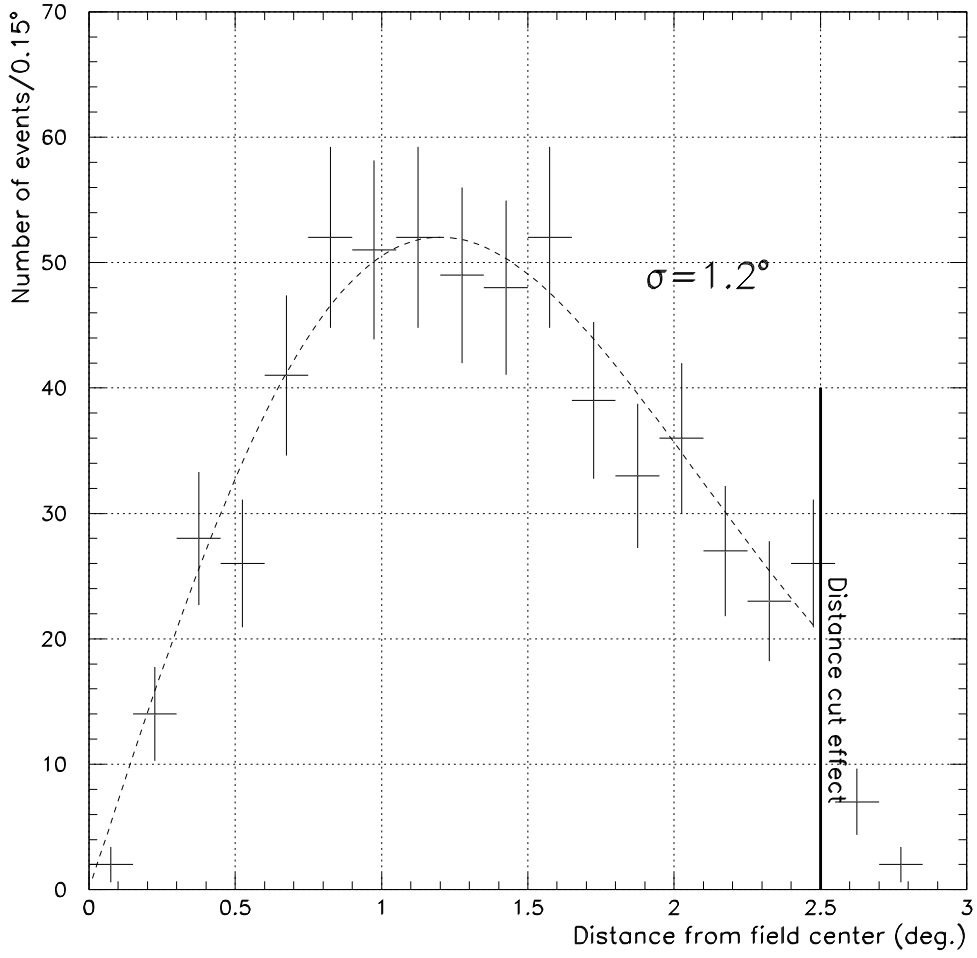


Fig. 2.— Radial distribution of the reconstructed arrival directions of simulated γ -rays with homogeneous arrival direction. The distribution is compared with the radial distribution of a two dimensional Gaussian with a standard deviation of 1.2° . The image centroid *distance* cut at 1.8° prevents reconstruction of events further than 2.5° away from the field center.

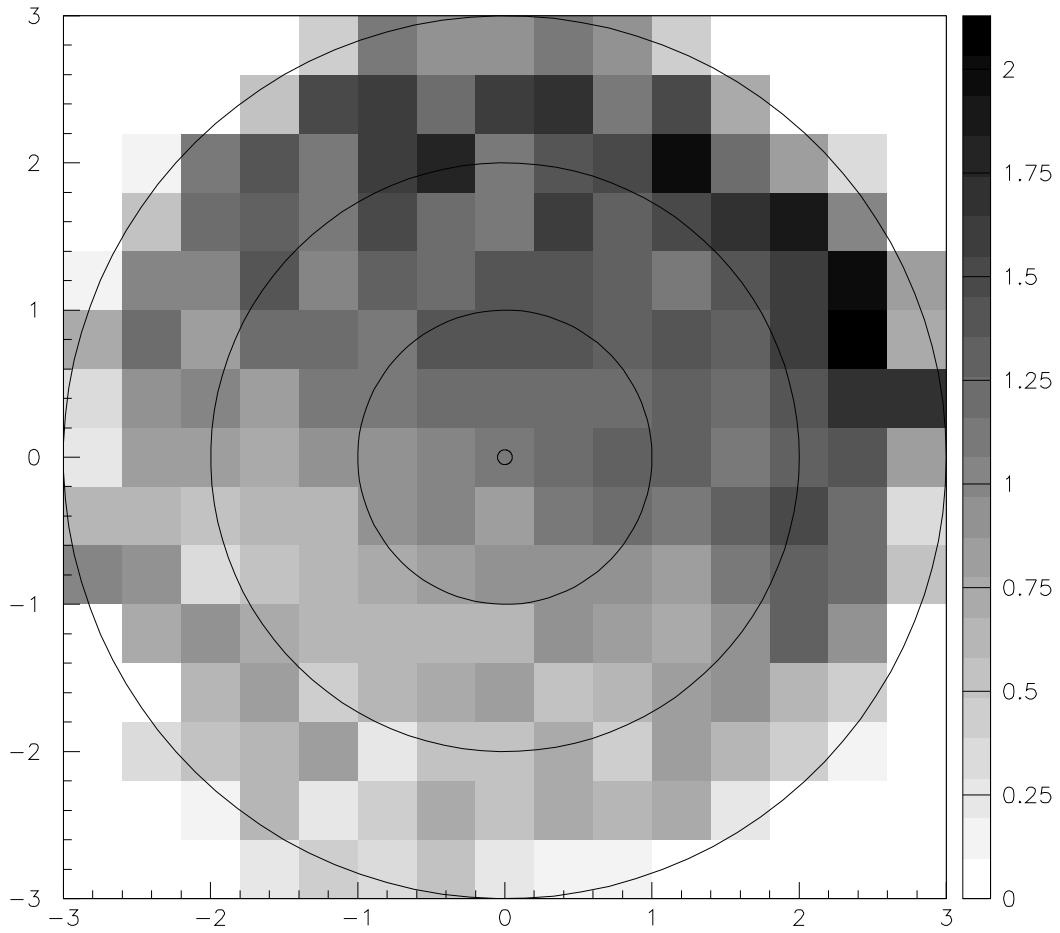


Fig. 3.— The sensitivity correction factor $S_{correct}$ is the ratio between the sensitivity inferred from simulation and the sensitivity to γ -ray like background events. This figure represent the camera frame map of $S_{correct}$ obtained from the 1999 OFF-source galactic plane observation.

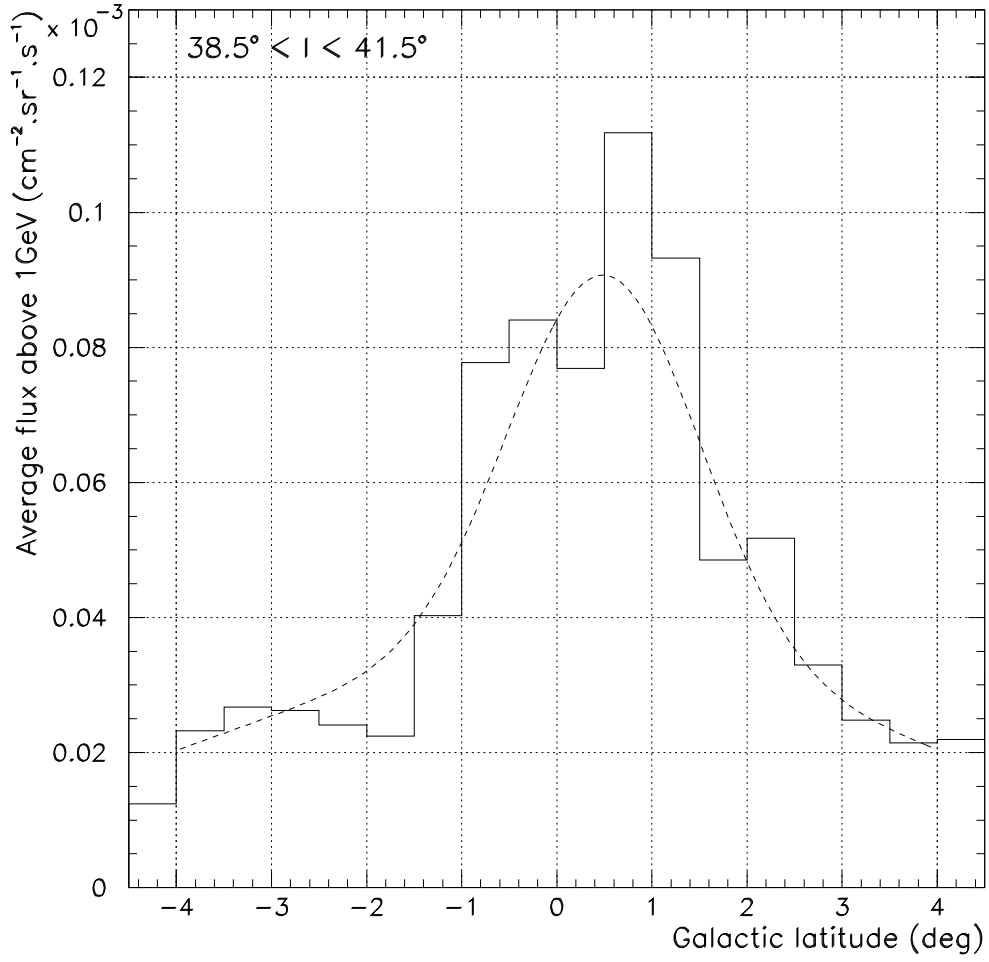


Fig. 4.— Average diffuse emission latitude profile between the galactic longitude $l = 38.5^\circ$ and $l = 41.5^\circ$ as observed by EGRET at energies $E > 1$ GeV. The smooth curve indicates how the distribution was modeled for the diffuse emission simulation above 500GeV.

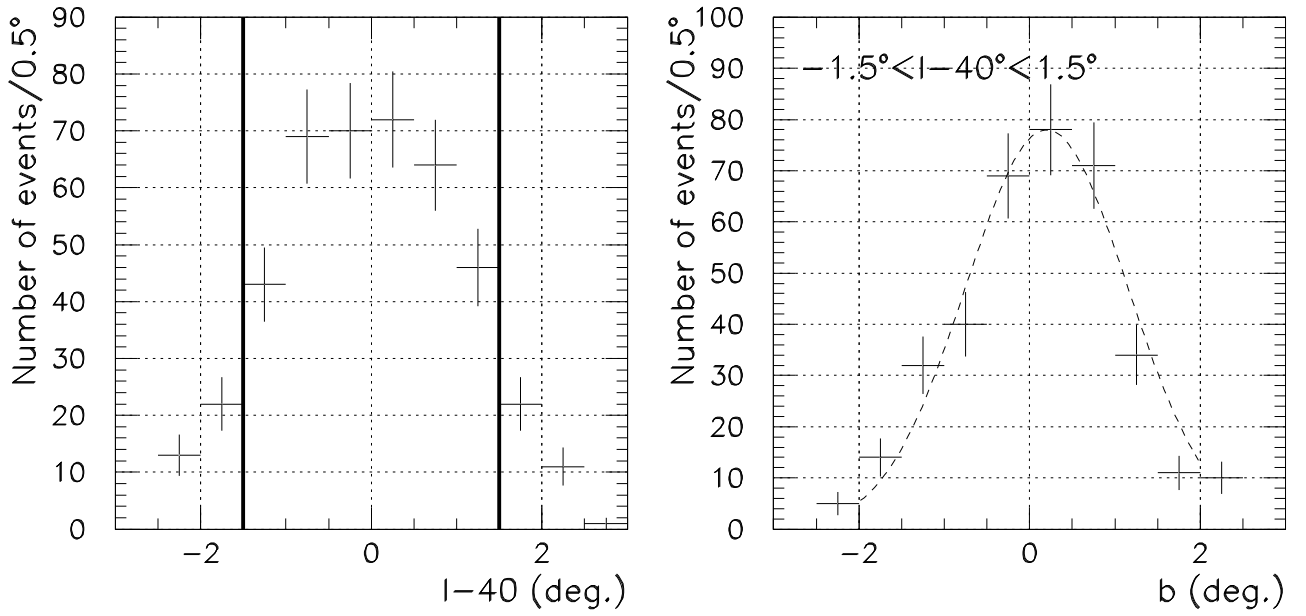


Fig. 5.— Distribution of the reconstructed direction of origin for the simulated TeV diffuse emission when projected on the galactic equator (left) and on the meridian (right). This distribution is obtained after all the selection criteria have been applied. The two vertical lines on the left histogram indicate the longitude selection criteria.

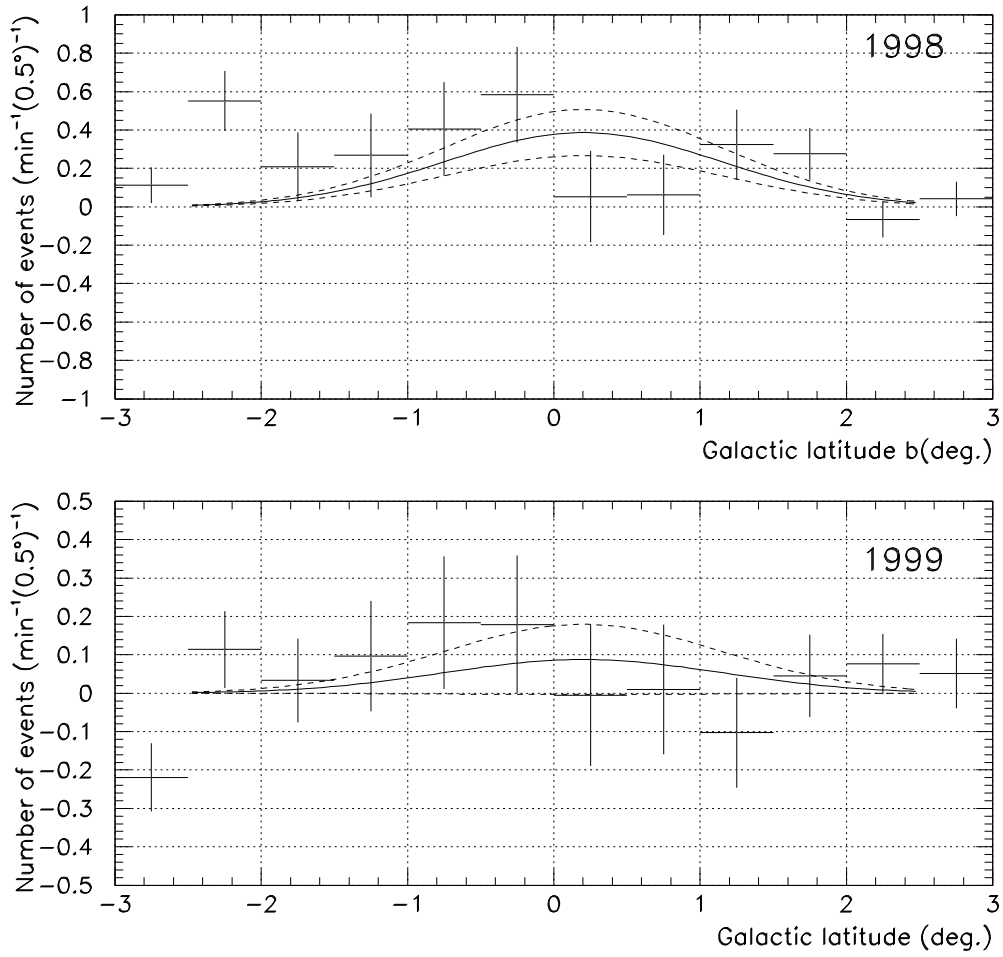


Fig. 6.— Latitude distribution of the excess observed in 1998 (top) and 1999 (bottom). The smooth solid curve shows the modeled simulated latitude profile when fitted to the data with amplitude as the only free parameter. The smooth dashed lines correspond to one standard deviation about the best fit.

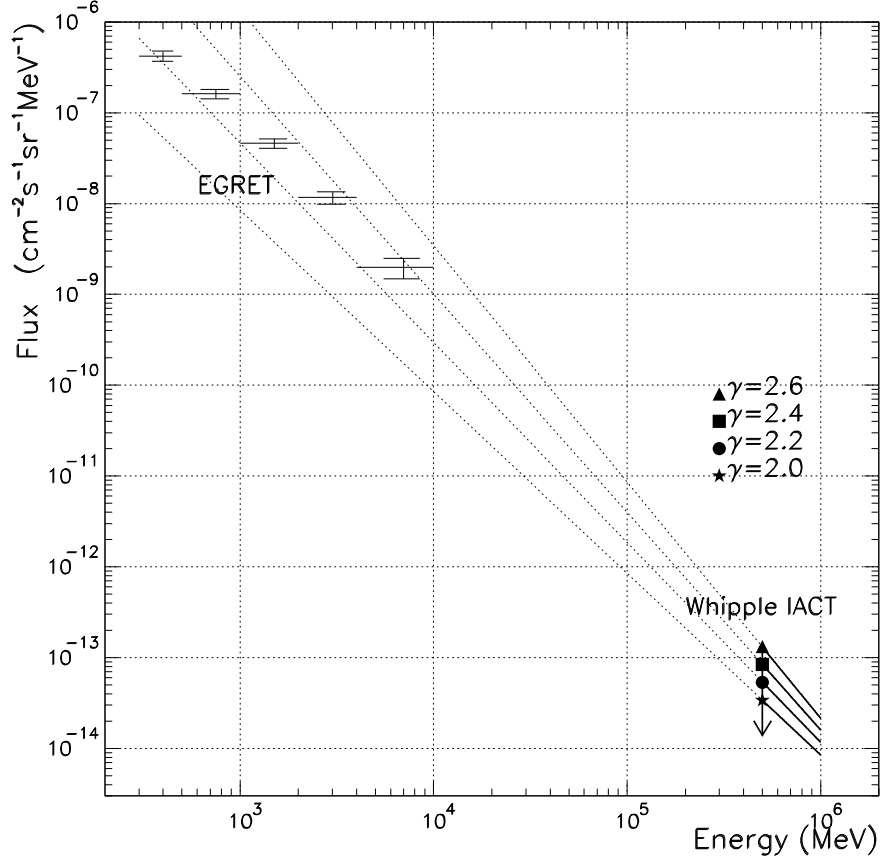


Fig. 7.— The EGRET differential spectrum of the diffuse emission observed in the portion of sky defined by $38.5^\circ < l < 41.5^\circ$ and $2^\circ < b < 2^\circ$ is compared to the upper limits obtained above 500 GeV in 1999 with the Whipple Telescope. The EGRET data points in the upper left of the figure with the 1σ error bars on flux are shown. The 99.9 % CL Whipple upper limits are shown in the lower right of the figure for assumed values of 2.0, 2.2, 2.4 and 2.6 (star, circle, square and triangle) for the differential spectral index γ . If these upper limits are extrapolated back to EGRET energies assuming a simple power law spectrum, the four dotted lines shown are obtained. It is then apparent that, if γ were less than about 2.2, a TeV signal should have been detected. The various dotted lines show a power law extrapolation down to the EGRET regime of our upper limits. Each line corresponds to a different assumption for the differential spectral index. The upper limit obtained with the smallest spectral index is not compatible with the flux recorded by EGRET above 1 GeV.

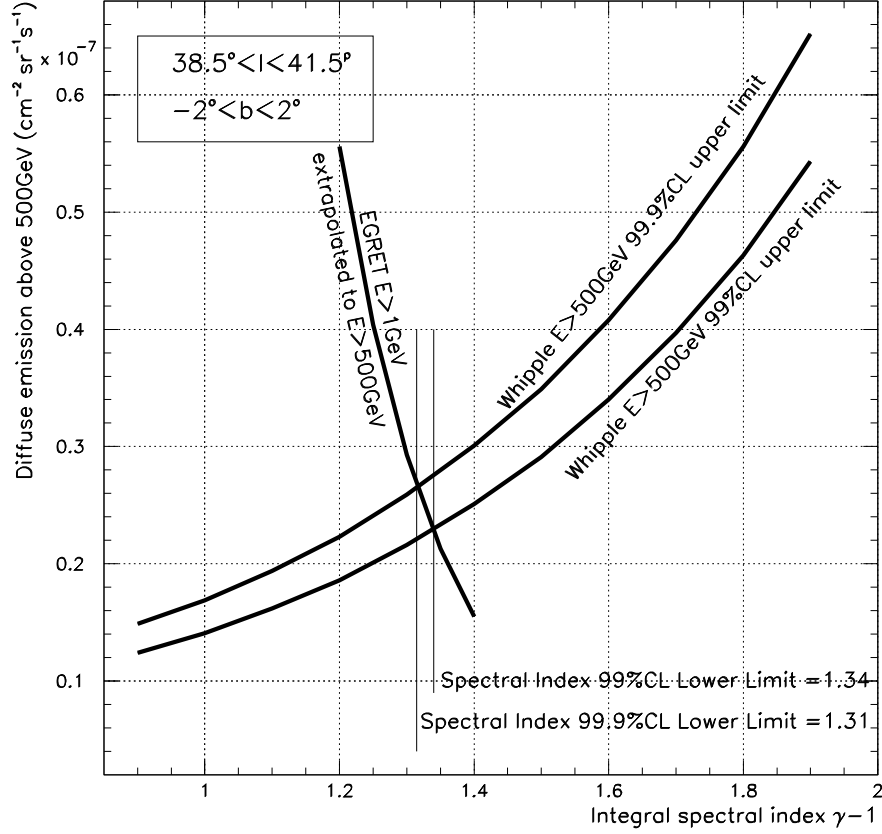


Fig. 8.— Diffuse emission upper limits derived from 1999 observations represented as a function of the assumed integral spectral index and compared with the flux measured by EGRET above 1 GeV in the same field and extrapolated to 500 GeV with various spectral indices. This comparison yields a lower limit (99.9% confidence level) for the integral spectral index of 2.31.